Fermi National Accelerator Laboratory

FERMILAB-Pub-97/426-E
E862

Measuring the Antihydrogen Lamb Shift with a Relativistic Antihydrogen Beam

G. Blanford et al.
The E862 Collaboration

Fermi National Accelerator Laboratory
P.O. Box 500, Batavia, Illinois 60510

December 1997

Submitted to *Physical Review D*

Operated by Universities Research Association Inc. under Contract No. DE-AC02-76CH03000 with the United States Department of Energy

Disclaimer

Distribution

Measuring the Antihydrogen Lamb Shift with a Relativistic Antihydrogen Beam

G. Blanford, K. Gollwitzer, M. Mandelkern, J. Schultz, G. Takei, and G. Zioulas
University of California at Irvine, Irvine, California

D. C. Christian
Fermilab, Batavia, Illinois

C. T. Munger
Stanford Linear Accelerator Center, Stanford University, Stanford, California 94309

(December 18, 1997)

We propose an experiment to measure the Lamb shift and fine structure (the intervals $2s_{1/2} - 2p_{1/2}$ and $2p_{1/2} - 2p_{3/2}$) in antihydrogen. A sample of 5000 antihydrogen atoms at a momentum of 8.85 GeV/c suffices to measure the Lamb shift to 5% and the fine structure to 1%. Atomic collisions excite antihydrogen atoms to states with $n = 2$; field ionization in a Lorentz-transformed laboratory magnetic field then prepares a particular $n = 2$ state, and is used again to analyse that state after it is allowed to oscillate in a region of zero field. This experiment is feasible at Fermilab.

11.30.Er, 25.43.+t, 36.10.-k

I. INTRODUCTION

The CPT theorem predicts the existence of the antimatter counterpart of every physical state. Antimatter states corresponding to elementary particles and some light nuclei have been observed. Until recently no antimatter atomic or molecular state had been detected. A CERN group [1] reported antihydrogen candidates in 1995. We have obtained a background-free sample of antihydrogen atoms in a Fermilab experiment [2]. Study of antimatter-matter symmetry is interesting as the only test of CPT invariance, a principle that is fundamental to our description of elementary particle interactions.

CPT invariance states that the product of the charge conjugation (C), parity (P) and time reversal (T) operations is an exact symmetry of nature. It is the minimal condition for the existence of antiparticles within quantum field theory. It can be derived from very general principles, specifically that a quantum field theory should be constructed from fields that belong to finite-dimensional representations of the Lorentz group, have local interactions invariant under the proper Lorentz group, and be described by a Hermitian Lagrangian. The predictions of the CPT theorem are that particle and antiparticle states have equal masses, spins, and lifetimes, and equal but opposite charges and magnetic moments. The most stringent tests made to date are the equality of the electron and positron g factors [3] to 2.1 parts in 10^{12}, and the equality of $|e/m|$ for the proton and antiproton [4] to 1.5 parts in 10^9. An indirect determination [5] of the K^0–$\bar{K}^0$ fractional mass difference yields a limit of $9{\cdot}10^{-19}$. Matter-antimatter symmetry has thus been studied in leptons and bound states of quarks. Using antimatter atoms, we can perform CPT tests of systems comprised of multiquark states (nuclei) interacting electromagnetically with leptons (electrons).

The hydrogen atom is the best studied of all physical systems and extremely precise measurements of its spectrum have been made, the best of which is of the $1s$–$2s$ interval [6] to 3.4 parts in 10^{13}. Antihydrogen at rest would be the ideal system for the study of CPT in atomic interactions and experiments are planned at CERN, where a new facility [7] is in construction, to emulate the high precision measurements made in hydrogen.

We have developed a way to measure the spectrum that uses instead antihydrogen in a relativistic atomic beam. Our method of measuring the energy differences between the $n = 2$ levels is an exact analog to the method of measuring the K_L–K_S mass difference by studying the time dependence of K^0 semileptonic decays. We describe an experiment which is feasible at the Fermilab Antiproton Accumulator with an antihydrogen beam at 8.85 GeV/c. The simulation described below is based on the parameters of that machine.

II. OVERVIEW OF EXPERIMENT

In our Fermilab experiment [2] we formed antihydrogen atoms by passing antiprotons stored in the Fermilab Antiproton Accumulator through a hydrogen gas jet target. We identified antihydrogen atoms, with no background, by requiring a coincidence between a positron signal and an antiproton tracked in a high-resolution ($5{\cdot}10^{-4}$) magnetic spectrometer. We now propose to pass the antiprotons through a high-Z gas jet target in order to take advantage of the Z^2 rise [8,9] in the cross section. Antihydrogen atoms will be identified using a coincidence between an antiproton tracked in a similar magnetic spectrometer and a positron tracked in a lower resolution detector.

Antihydrogen atoms emerge from the Accumulator in the $1s$ state. The atoms are next excited by their passage through a thin foil mounted in a magnetic field. The electric field experienced by the atoms in their rest frame ionizes all of the excited states except those in the long-lived Stark level with $n = 2$. A long-lived state can be represented as a coherent sum of the zero-field $n = 2$ states, which are split by the fine structure and Lamb shift. The atoms next pass through a region with zero magnetic field, in which the state accrues phase differences between its zero-field components, resulting in "vacuum regeneration" of the medium-lived and short-lived Stark states. The reappearance of these states changes the point where the atom will ionize in a second magnet, since the short- and medium-lived states ionize in smaller magnetic fields. By measuring where the atoms ionize, as a function of the flight distance in zero field, we can determine the fine structure and Lamb shift splittings. The ionization point may be found by tracking the positron and antiproton.

III. METHOD

In a strong electric field the 8 states with $n = 2$ separate into 3 Stark levels, each of which has a different rate of field ionization. At fields large enough that the rates of field ionization are much larger than the rate ($6.27{\cdot}10^8\,\mathrm{s}^{-1}$) at which the $2p$ state decays radiatively, the lifetimes of the levels are in the ratios of roughly 25:5:1. We will label these levels and the states that belong to them as long, medium, and short, respectively. The difference in the lifetimes allows us to pass a beam of atoms with $n = 2$ through an electric field and cause all but the long level to ionize.

If this beam passes suddenly into a 'drift' region of zero field, a surviving long state projects onto the zero-field eigenstates as

$$\Psi(t{=}0) = \sqrt{\tfrac{1}{2}}|s_{1/2}\rangle + \sqrt{\tfrac{1}{6}}|p_{1/2}\rangle - \sqrt{\tfrac{1}{3}}|p_{3/2}\rangle\,. \qquad (1)$$

The state then evolves forward in time as

$$\begin{aligned}\Psi(t) = &\sqrt{\tfrac{1}{2}}e^{-iE(s_{1/2})t/\hbar}|s_{1/2}\rangle \\ &+\sqrt{\tfrac{1}{6}}e^{-iE(p_{1/2})t/\hbar-(\Gamma/2)t/\hbar}|p_{1/2}\rangle \\ &-\sqrt{\tfrac{1}{3}}e^{-iE(p_{3/2})t/\hbar-(\Gamma/2)t/\hbar}|p_{3/2}\rangle\,. \qquad (2)\end{aligned}$$

Here Γ is the width (fwhm) of the $2p$ state due to its radiative decay.

The state that is pure long at $t = 0$ evolves into a superposition of long, medium, and short. If the beam suddenly enters another electric field, this superposition is again projected onto the Stark states. A state with a large projection onto long will typically penetrate deeply into the second electric field before ionizing; a state with a large projection onto short will typically ionize immediately; and a state with a large projection onto medium will usually ionize at an intermediate depth. By measuring the distribution of the depth at which the state ionizes, as a function of the time spent in zero field, we can determine the zero-field splittings of the $n = 2$ states.

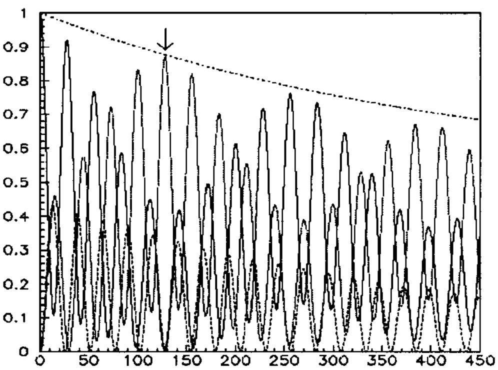

FIG. 1. Plot of the probability that an initial long state is found in the long (solid), medium (dashed), or short (dotted) level as a function of the flight distance in cm in zero field. The sum of the three probabilities (dash-dot) shows the decline due to radiative decay. Note that a state that was pure long at $x = 0$ is almost pure short (arrow) at $x = 128$ cm, when only 12% of the states have decayed.

The probabilities that an initial long state may be found in a long, medium, or short state are

$$P\begin{pmatrix}\text{long}\\ \text{short}\end{pmatrix} = \left[\tfrac{1}{2} \pm e^{-x/2}\left(\tfrac{1}{3}\cos fx + \tfrac{1}{6}\cos lx\right)\right]^2 + \left[e^{-x/2}\left(\tfrac{1}{3}\sin fx - \tfrac{1}{6}\sin lx\right)\right]^2 \qquad (3)$$

and

$$P(\text{medium}) = \tfrac{2}{9}e^{-x}\left(1-\cos(f+l)x\right)\,, \qquad (4)$$

where $x = \Gamma t/\hbar$ and

$$\begin{aligned} l &= \left(E_{s_{1/2}} - E_{p_{1/2}}\right)/\Gamma > 0\,; \quad \text{and} \\ f &= \left(E_{p_{3/2}} - E_{s_{1/2}}\right)/\Gamma > 0\,. \qquad (5)\end{aligned}$$

These oscillating functions are plotted in Fig 1. The fast oscillation, of period 28.5 cm, in the probability of a long state is due to the $2s_{1/2} - 2p_{3/2}$ splitting, and the slow modulation, of period 267 cm, is due to the Lamb shift splitting. Since the long state can oscillate into a virtually pure short state, and since the ionization rates of these states differ by a factor of roughly 25, the oscillation is easy to detect.

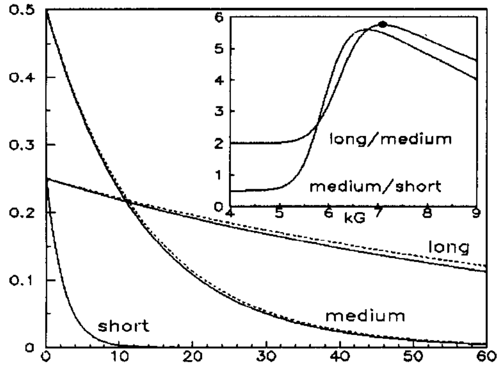

FIG. 2. Plot of the probabilities that an incoherent mixture of $n = 2$ states is found in the short, medium, or long level, as a function of the flight distance in cm in a transverse laboratory magnetic field of 7.090 kG. The solid curves show the result of the full simulation; the dashed curves show the result in the approximation that the three levels decay separately with decay rates set by field ionization alone. The difference can be perceived only for the medium and long states; it is due almost entirely to the omission of the appropriate fraction (1/2, 1, or 1/2) of the $2p$ radiative decay rate appropriate for each of the three levels. At the field of 7.090 kG ratio of the decay length of long to that of medium has its maximum value of 5.8 (insert).

We now analyze a design for an experiment where the large ($\sim 2{\cdot}10^9$ V/cm) electric fields required are provided by the Lorentz transform of laboratory magnetic fields into the rest frame of an 8.85 GeV/c antihydrogen beam, such as has been produced at FNAL [2].

Accurate calculations are required of the rates of field ionization for the different levels with $n = 2$. The eigenvalue problem for the Schrödinger hydrogen atom in an electric field (nearly) separates in parabolic coordinates; the ionization rates have been intensively studied theoretically and are available to 6 decimals at discrete values of the electric field [10]. They are also available as (asymptotic) series in powers of the applied field, times an exponential factor; while not convergent, these series [11] allow accurate interpolation. The code used in our simulations evolves the 8×8 density matrix for the states with $n = 2$ through the perpendicular electric and magnetic fields that result from the Lorentz transform of a transverse laboratory magnetic field. The Wigner-Weisskopf formalism is used to include the losses due to field ionization and to radiative decay; the linear [12] Stark and Zeeman perturbations are included, as are the fine-structure and Lamb shift splittings, but the hyperfine splitting is neglected.

We begin the experiment by making antihydrogen atoms by circulating an antiproton beam stored in the Fermilab Antiproton Accumulator through a high-Z gas jet. The atoms emerge from the Accumulator in the $1s$ state, and roughly 8% of the atoms are excited [13] to states with $n = 2$ by passing them through a very thin ($60\,\mu$gm/cm^2) carbon or equivalent polypropylene foil, while most of the other atoms remain in the $1s$. The $1s$ atoms are ionized in a second, thicker foil far downstream and counted to monitor the relative luminosity.

We assume that collisions in the foil produce the eight $n = 2$ states with equal probability [14]. The subsequent evolution of these states in a uniform, transverse magnetic field of 7.090 kG is shown in Fig. 2. The medium [15] and short states ionize rapidly, leaving a nearly pure long state. The ionization rates are sensitive functions of the applied magnetic field and the beam momentum. Changing either by 0.1% will change the $1/e$ lengths for ionization in this magnet by 1.8%. The unusual sensitivity arises because field ionization is a tunneling process and so its rate varies exponentially with the applied electric field. This sensitivity does not pose a problem because the momentum of the Accumulator is controlled to 0.02%.

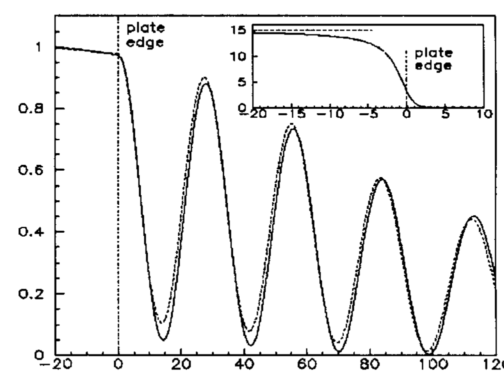

FIG. 3. The probability as a function of coordinate y [cm] that a state that is pure long at $y = -20$ cm remains long as it passes into the drift region. The field profile used (insert) is that of a transverse field of 15 G that is screened by a pair of parallel, infinitely permeable plates that have their edges at $y = 0$ and are separated by 4 cm. (It is convenient to study the field from a pair of plates, instead of from a cylinder, because the profile may be obtained in almost closed form [21] by conformal mapping.) The solid curve is the result of the full simulation; the dashed curve is the approximation that for $y < 0$ the long state does not mix and may only decay radiatively, and at $y = 0$ begins to oscillate in zero field as given by Eq. (3).

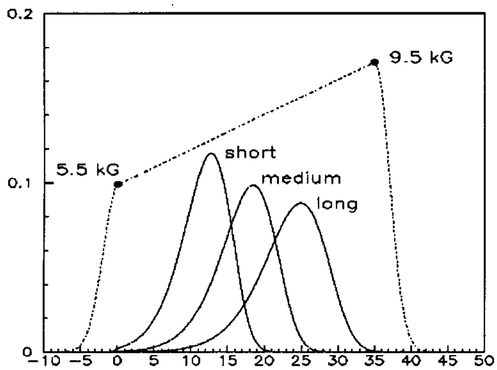

FIG. 4. The probability distribution $dP/dy\,[\mathrm{cm}^{-1}]$ for the ionization in the second magnet of a short, medium, or long state, as a function of the depth y in cm. The field profile of the magnet is shown as the dashed line. The total probabilities that a short, medium, or long state ionizes in the magnet are respectively 0.976, 0.942, and 0.963. A long state ionizes with greater probability than does a medium state, though a long state has further to fly before it ionizes, because it has half the rate of radiative decay.

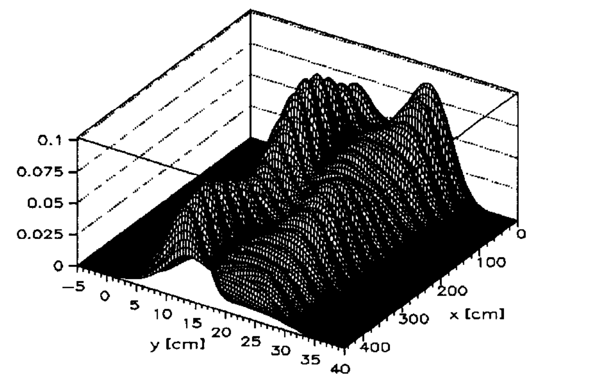

FIG. 5. The differential probability $dP/dy\,[\mathrm{cm}^{-1}]$ for a positron to appear at coordinate y in the second magnet, as a function of the drift distance x in cm. The fast oscillation (period 28.5 cm) is due to the $2s_{1/2}{-}2p_{3/2}$ oscillation, while the slow modulation in its amplitude (period 267 cm) is due to the $2s_{1/2}{-}2p_{1/2}$ oscillation. The overall loss in probability with increasing x is due to radiative decays in the drift region, which produce atoms in the $1s$ state that consequently do not ionize in the second magnet.

In the drift region, laboratory transverse magnetic fields must be $\leq 3\,\mathrm{mG}$ to avoid Stark mixing. Longitudinal magnetic fields involve only the weaker Zeeman mixing and are not boosted and so can be much larger, $\leq 10\,\mathrm{G}$. A sufficiently field-free region of adjustable length can be provided by a set of telescoping μ-metal cylinders.

The transition from the first magnet to the drift region must now be tailored so that the $n = 2$ Stark states undergo a non-adiabatic transition. A key observation is that in a field below 5 kG the $n = 2$ states do not ionize (see Fig. 4); and in a field above 3 G the Stark splitting is so much larger than the fine structure splitting that the long, medium, and short states do not mix. It is only in the range 3 G to 3 mG that a sudden fall of the magnetic field must be engineered; qualitatively we expect that the fields must be made to fall off in a distance short compared to the spatial period of the fine-structure oscillation, or 28.5 cm. Figure 3 shows how the transition can be made non-adiabatic using a simple structure that is large enough to accommodate the antihydrogen beam.

For a second magnet, Fig. 4 shows the separate probability distributions for the point of ionization of the short, medium, and long states. The distribution of ionization points is shown as a function of drift distance in Fig. 5. An antihydrogen atom ionizes into an equal-velocity positron and antiproton, both of which we track to determine the ionization point. Gulley *et al.* [16] used a similar technique to ionize and count states with $n \geq 3$ in an 800 MeV neutral hydrogen beam.

We simulate an experiment by integrating luminosity sufficient for 100 long states, on average, to emerge from the first magnet. The $1/e$ decay length of the $2p$ state sets a natural limit [17] to the useful length of a drift region, and we wish to sample a set of drift distances separated by substantially less than the spatial period of the fine structure oscillation. Accordingly we divide the luminosity evenly between 101 equally spaced drift distances ranging from from 0 to 450 cm. An average of 80 ionizations occur. The complicated function shown in Fig. 5 is fit to the data using the Method of Maximum Likelihood [18]. In keeping with the results of the Fermilab experiment, we assume that there is no background. There are three variables fit: the shifts of the $2s_{1/2}$ and $2p_{1/2}$ states toward the $2p_{3/2}$ state, relative to their values in hydrogen; and the number of long states that emerge from the first magnet.

Shown in Fig. 6 are the results of the fit for 20 simulated experiments. The experiment is sensitive at the 1σ level to independent shifts of either the $2s_{1/2}$ or the $2p_{1/2}$ state equal to 0.5 and 0.9 radiative widths of the $2p$ state. Equivalently, the experiment measures the antihydrogen Lamb shift (the $2s_{1/2}{-}2p_{1/2}$ splitting) to 5% and the fine structure (the $2p_{1/2}{-}2p_{3/2}$ splitting) to 0.9%. Assuming that an interaction that violates CPT will shift the $2s$ state but not the $2p$, the experiment is sensitive to a

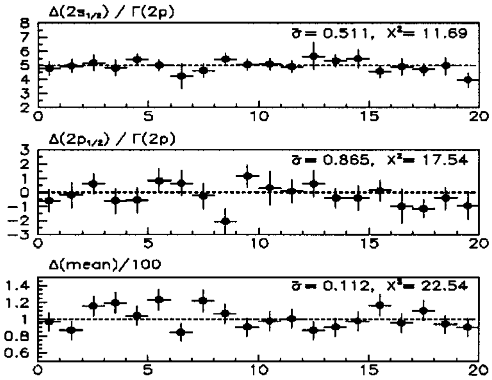

FIG. 6. Results of a three-parameter likelihood fit to 20 simulated experiments that measure the fine structure and Lamb shift of antihydrogen. Shown are the shifts toward the continuum of the $2s_{1/2}$ and $2p_{1/2}$ states, relative to their values in hydrogen, in units of the $2p$ radiative width. Shown too is the ratio of the number of long states let into the drift region to the set value of 100. The vertical error bars are the standard 1-sigma errors estimated for each variable y from the value of $\partial^2 \ln L/\partial y^2$ evaluated at the minimum. Dashed lines show the values set in the simulation; a CPT-violating shift of the $2s_{1/2}$ state of +5 is identified cleanly.

shift of $5{\cdot}10^{-8}$ of the $2s$ binding energy.

It is at first sight surprising that so small a number of detected events suffices to determine the energy splittings precisely. We model this effect by using the likelihood method to form an estimate ω of a true frequency ω' from N events distributed as $1{+}\cos(\omega' t)$ over a time interval T. The log of the expectation value of the likelihood function in this simple model can be found analytically, and for $N = 1$ equals

$$\log L = \log\left[1 + \frac{\sin\omega T}{\omega T} + \frac{\sin\omega' T}{\omega' T} + \frac{\sin(\omega+\omega')T}{2(\omega+\omega')T} + \frac{\sin(\omega-\omega')T}{2(\omega-\omega')T}\right] - \log\left[1+\frac{\sin\omega T}{\omega T}\right] - \log\left[1+\frac{\sin\omega' T}{\omega' T}\right] . \quad (6)$$

This function is plotted as a function of ω in Fig. 7. It oscillates about a central minimum at the expected value with a separation of the central and adjacent local minima of $3\pi/T$. The rms uncertainty σ_ω is found from the expectation of the second derivative of $-\log L$ and is given by

$$\frac{\sigma_\omega}{\omega} = \left[\frac{3}{N}\frac{1}{\left((2\pi k)^2 - 9\right)}\right]^{1/2} . \quad (7)$$

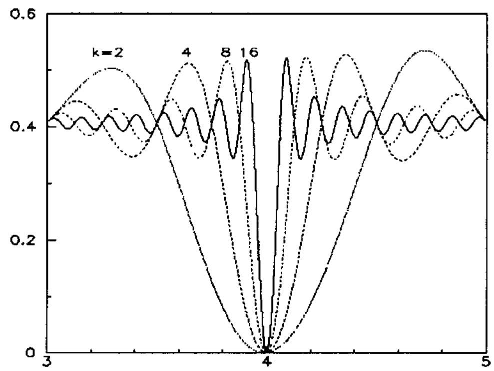

FIG. 7. The (negative) log of the expectation value of the likelihood function for 1 event distributed as $1+\cos(\omega' t)$ over a time T. The plots are shown as a function of the estimate ω for the parameter $\omega' = 4$, for $T = 2\pi k/\omega'$ where k is an integer. The curves are shifted vertically to have the common value 0 at their common global minimum at $\omega = 4$. The width of the central minimum scales as $1/k$.

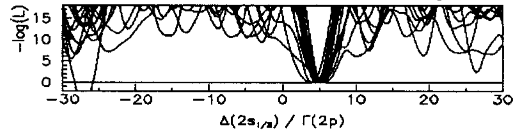

FIG. 8. The (negative) log-likelihood function near the minimum, plotted as a function of the shift of the $2s_{1/2}$ state towards the continuum in units of the $2p$ radiative width. Each figure shows functions for different experiments with the same number of long states entering the drift region; the functions are shifted vertically so that they have the common value zero at the local minimum nearest the preset CPT-violating shift of +5. The third figure shows the functions for the same 20 simulated experiments as in Fig. 6.

Here $k = \omega' T/2\pi$ is the number of periods over which observation extends. For $k = 1$ and $N = 100$, we find that σ_ω/ω is 3%, roughly equal to the error we have simulated for the Lamb shift. The resolution improves as $1/T$ for a fixed number of events because of the increasing lever arm by which each event constrains the phase of the oscillation. For $k = 16$ we find that σ_ω/ω is 0.2%, roughly equal to the error we have simulated for the fine structure. An experiment must have a sufficient number of events N to resolve the central minimum.

For the antihydrogen experiment we similarly obtain adjacent local minima in the (negative) log-likelihood function that may lead to a spurious fit for a sufficiently small number of events. The effect of these minima on the 20 simulated experiments, and on experiments with yet smaller expected numbers of events, is examined in Fig. 8. Experiments with 100 long states expected are almost always free of such extra minima; experiments with 40 are usually free, while experiments with as few as 20 often have such minima, and moreover will often lack the statistical power to exclude the possibility of no shift of the $2s$ state if in fact a shift is present. Demanding 100 long states for a practical experiment therefore seems reasonable, since an experiment may still succeed if only 40 are produced. Given that 8% of an antihydrogen beam in the $1s$ state may be excited by collisions in a foil to states with $n = 2$, and that $1/4$ of these are long states, we assert that an experiment can be done on a sample of 5000 atoms of antihydrogen.

IV. EXPERIMENTAL MATTERS

A. Rate

Antihydrogen is formed in antiproton-nucleus collisions by the process $\bar{p}Z \rightarrow Z\bar{H}e^-$. We have measured [2] the cross section at 5.7 GeV/c for $Z = 1$ to be $1.12 \pm 0.14 \pm 0.09$ pb. The cross section for forming antihydrogen in the $1s$ state at 8.85 GeV has been estimated [8,9] to lie between $1.5Z^2$ and $5.0Z^2$ pb; for Xenon the lower estimate gives 4.4 nb. The design of the Accumulator allows antihydrogen formed in states with $n = 2$ to contribute to the flux of $1s$ antihydrogen from the machine, increasing the effective cross section by another $\sim 13\%$ to 4.9 nb. The beam antiprotons also interact by inelastic processes and by large-angle elastic scattering, both resulting in immediate beam loss, and by multiple small-angle elastic scattering. This multiple scattering increases the size and momentum spread of the beam and leads to beam loss when this beam "heating" exceeds the cooling capability of the machine. We take a gas jet density such that, at the FNAL Antiproton Accumulator, there are no beam losses due to heating, giving an instantaneous luminosity of approximately $10^{29}\,\mathrm{cm}^{-2}\mathrm{sec}^{-1}$. We estimate the effective Xe cross section for beam loss at this machine to be 3 b so that 1.6 antiprotons per 10^9 consumed result in antihydrogen. The Accumulator is expected to stack antiprotons at 10^{11} per hour during Fermilab Collider Run 2. At the above luminosity we consume 1% of these antiprotons, giving in parasitic operation ~ 40 antihydrogen atoms per day. Of these 8% are excited to $n = 2$ of which $1/4$ are in a long state, giving 0.8 atoms in a long state per day. Accumulating the needed 100 long states takes four months of running. Electron cooling, which delivers far greater cooling power, is planned for the Fermilab Recycler [19]. It may be possible to operate with much greater luminosity in that machine.

The FNAL Antiproton Accumulator is able to circulate protons in the direction opposite to the normal circulation of antiprotons. Relativistic atoms of hydrogen are formed not only by the reaction $pZ \rightarrow ZHe^+$ but by the radiative capture of a target electron, a process which has the relatively large cross section [20] of 344 pb at 8.85 GeV/c. By moving the experiment and reversing the polarity of its magnets, the Lamb shift and fine structure splittings of hydrogen can be measured by the same apparatus as that used for antihydrogen. Such an experiment would be useful in analyzing possible systematic effects.

B. Event detection

The Fermilab experiment [2] demonstrated that observation of an antiproton track within $1 \cdot 10^{-2}$ of the Accumulator momentum, in coincidence with a positron, detects antihydrogen with no background. As in that experiment, the antiproton is detected in a magnetic arm instrumented with 1 mm wire chambers with a momentum resolution of $5 \cdot 10^{-4}$. The 4.8 MeV/c positron is detected in a thin, vertical detector with coordinate sensitivity in the beam direction, positioned in the second magnet about 2 cm from the beam axis. At FNAL, the antihydrogen beam is contained (95%) in a circle of 1 cm radius. The positron, emerging from the ionization point in the beam direction, orbits with a cyclotron radius of about 2 cm in the horizontal plane and so traverses the detector twice, the midpoint of the hits giving the longitudinal coordinate of the ionization with a precision of 1 mm rms. A multiwire proportional chamber with windows and cathodes made of 25 micron aluminized mylar ($\sim 5 \cdot 10^{-5}$ radiation lengths) is a suitable detector. Straw tubes, silicon-strip detectors and scintillating fibers are alternative technologies. The antiproton track furnishes the horizontal distance between the point of ionization and the positron detector to better than 1 mm rms, giving an additional constraint. A poorer measurement of the longitudinal coordinate of the ionization point (1 cm rms) comes from the antiproton track, limited by the 0.2 mr divergence of the antihydrogen beam.

V. CONCLUSIONS

We describe an experiment to measure the Lamb shift and fine structure (the intervals $2s_{1/2} - 2p_{1/2}$ and $2p_{1/2} - 2p_{3/2}$) in antihydrogen. In four months of parasitic operation at the FNAL Antiproton Accumulator, these intervals can be measured to 5% and 1% respectively.

This work was partially supported by the U. S. Department of Energy.

---

[1] G. Baur, G. Boero, S. Branksiepe, A. Buzzo, W. Eyrich, R. Geyer, D. Grzonka, J. Hauffe, K. Kihan, M. LoVetere, M. Macri, M. Mossburger, R. Nellen, W. Oelert, S. Passagio, A. Pozzo, K. Rohrich, K. Sachs, G. Schepers, T. Sefzick, R. S. Simon, R. Stratmann, F. Stinzig, and M. Wolke, Phys. Lett. **B368**, 251 (1996).

[2] G. Blanford, D. C. Christian, K. Gollwitzer, M. Mandelkern, C. T. Munger, J. Schultz, and G. Zioulas, submitted to Phys. Rev. Lett.

[3] R. S. Van Dyck, Jr., P. B. Schwinberg, and H. G. Dehmelt, Phys. Rev. Lett. **59**, 26 (1987).

[4] G. Gabrielse, D. Phillips, W. Quint, H. Kalinowsky, G. Rouleau, and W. Jhe, Phys. Rev. Lett. **74**, 3544 (1995). Note the number in equation 2 should read 0.999 999 998 5(11); see [5], p. 561.

[5] The Particle Data Group, Phys. Rev. D **54**, 1 (1996); see p. 412.

[6] Th. Udem, A. Huber, B. Gross, J. Reichert, M. Prevedelli, M. Weitz, and T. W. Hänch, Phys. Rev. Lett. **79**, 2647 (1997).

[7] Design Report CERN/PS 96-43 (AR). See also http://www.cern.ch/PSdoc/acc/ad/index.html.

[8] C. A. Bertulani and G. Baur, "Antihydrogen production and accuracy of the equivalent photon approximation," HEPPH-9711273, Nov. 1997; e-Print Archive hep-ph/9711273.

[9] C. T. Munger, S. J. Brodsky, and I. Schmidt, Phys. Rev. D**49**, 3288 (1994); C. T. Munger, S. J. Brodsky, and I. Schmidt, Hyperfine Interactions **76**, 175 (1993).

[10] R. J. Damburg and V. V. Kolosov, J. Phys. B **9**, 3149 (1976); see Table 2. R. J. Damburg and V. V. Kolosov, J. Phys. B11, 1921 (1978); again see Table 2.

[11] H. J. Silverstone, E. Harrell, and C. Grot, Phys. Rev. A **24**, 1925 (1981).

[12] In fields of about 7 kG the Stark effect mixes states with $n = 2$ and states with $n \neq 2$ substantially, and so including only the linear Stark and Zeeman effects is not adequate to find accurate eigenvalues. It is adequate for finding accurate decay rates, however, because the Stark splitting so dominates the fine structure, Lamb, and Zeeman splittings that the Stark states decouple. The error in the eigenvalues then appears only in irrelevant phase factors.

[13] B. Gervais, C. O. Reinhold, and J. Burgdörfer, Phys. Rev. A**53**, 3189 (1996). The $n = 2$ yield ($\sim 8 - 10\%$) and optimum target thickness for a beam kinetic energy of 800 MeV/c is estimated from Fig. 10. In the Born approximation all cross sections scale as $1/\beta^2$, so at 8.85 GeV/c the yield is the same and the target thickness merely greater by a factor of 1.4.

[14] We further assume that this remains so if the foil is in a 7 kG magnetic field, when the Stark effect mixes substantially states with $n = 2$ with states with $n \neq 2$. The cross sections for the various excitation, rearrangement, and ionization collisions may however be expected to change from their zero-field values. We may avoid making this further assumption by leaving the foil in zero field and putting the first magnet a short distance downstream.

[15] Half of the remaining medium states are the $2p_{3/2}$, $m_j = \pm 3/2$ states that do not oscillate in zero field and are unlikely to confuse the oscillating pattern of ionization that results from the long states.

[16] M. S. Gulley, P. B. Keating, H. C. Bryant, E. P. MacKerrow, W. A. Miller, D. C. Rislove, S. Cohen, J. B. Donahue, D. H. Fitzgerald, S. C. Frankle, D. J. Funk, R. L. Hudson, R. J. Macek, M. A. Plum, N. G. Stanciu, O. B. van Dyck, C. A. Wilkinson, and C. W. Planner, Phys. Rev. A**53**, 3201 (1996).

[17] As shown in Eqns. (3-4), the probability of an oscillation between long and short falls as $e^{-x/2}$, not e^{-x}. An experiment therefore may be able to use a drift region of order not once but twice the $1/e$ decay length of the $2p$ state, or 900 cm.

[18] R. Barlow, Nucl. Instrum. and Meth. in Phys. Res. A **297**, 496 (1990); J. Orear, University of California Report UCRL-8417 (1958). In keeping with standard numerical practice, we minimize the negative log-likelihood rather than maximize the log-likelihood.

[19] G. Jackson, FERMILAB-TM-1991, Nov., 1996.

[20] V. B. Berestetskii, E. M. Lifshitz, and L. P. Pitaevskii, Vol. 4 of "Quantum Electrodynamics, Course of Theoretical Physics," 2nd ed., (Pergamon, New York, 1982), pp. 207-216.

[21] N. Levinson and R. M. Redheffer, "Complex Variables," (Holden-Day, Inc., 1970), pp. 295-297.